



Comparison of Compression-After-Impact and Flexure-After-Impact protocols for 2D and 3D woven fiber-reinforced composites



Kevin R. Hart^{a,b}, Patrick X.L. Chia^a, Lawrence E. Sheridan^a, Eric D. Wetzel^c, Nancy R. Sottos^{b,d}, Scott R. White^{a,b,*}

^a Department of Aerospace Engineering, University of Illinois at Urbana-Champaign, 104 S. Wright St., Urbana, IL 61801, USA

^b Beckman Institute for Advanced Science and Technology, University of Illinois at Urbana-Champaign, 405 N. Mathews Ave., Urbana, IL 61801, USA

^c Weapons and Materials Research Directorate, US Army Research Laboratory, RDRL-WMM-A, Bldg. 4600, Aberdeen Proving Ground, MD 21005, USA

^d Department of Materials Science and Engineering, University of Illinois at Urbana-Champaign, 1304 W. Green St., Urbana, IL 61801, USA

ARTICLE INFO

Article history:

Received 4 January 2017
Received in revised form 30 June 2017
Accepted 2 July 2017
Available online 8 July 2017

Keywords:

Compression after impact
Impact behavior
Delamination
Mechanical testing

ABSTRACT

Post-impact mechanical response of 2D and 3D woven glass/epoxy composite plates and beams of equivalent areal density are evaluated using both Compression-After-Impact (CAI) and Flexure-After-Impact (FAI) testing protocols. Residual strength and stiffness for CAI and FAI are compared after normalization of impact energy with respect to specimen volume. Post-impact flexural strength and modulus from FAI testing exhibit larger reductions with respect to impact energy in comparison to CAI results. At the largest impact energies tested, FAI testing yields 70% reduction in flexural strength compared to only 20% reduction (in compressive strength). Architecturally, 3D woven composites retain greater post-impact mechanical performance as a result of the through-thickness Z-tow which suppresses delamination growth and opening during impact.

© 2017 Elsevier Ltd. All rights reserved.

1. Introduction

Fiber-reinforced composites possess exceptional specific mechanical properties and are now commonly used in applications requiring materials that are strong, stiff, and light. However, low-velocity out-of-plane impact damage severely compromises the load-carrying capability of these parts by introducing inter-ply delaminations, transverse matrix cracks, tensile cracks, and fiber rupture which may reduce the residual strength and modulus of the composite in tension, compression, and/or shear by up to 80% [1,2].

Evaluation of post-impact performance of composites has been dominated by the Compression-After-Impact (CAI) testing protocol, first utilized by NASA [3], the Composites Research Advisory Group (CRAG) [4], and Boeing [5] in the mid-1980s and later standardized by ASTM in 2005 [6]. The research literature on impact response of composites subject to the CAI protocol is vast, with multiple review articles encompassing: damage formation mechanisms during impact [2,7–14], critical strain energy release rates during impact [2,7,9,10,13–16], models of residual strength

and modulus as a function of impact energy [2,10,13–16], and the effects of constituents (matrix/fibers/interface) on residual mechanical properties [2,7,10,12,13,16]. Key findings from these studies reveal that fabric architecture, matrix toughness, interfacial treatments (silanes), void content, sample thickness, stacking sequence, impactor geometry, impactor velocity, compression testing rates, and boundary conditions associated with fixturing all have significant effects on the post-impact performance of the material.

Despite the wide-spread adoption of the CAI testing protocol, many researchers have criticized the sole use of CAI in evaluating post-impact performance because results are sensitive to clamping conditions, samples are limited to a specific thickness range, and only compressive properties are evaluated. As a result, alternate testing protocols have been investigated for post-impact evaluation of mechanical properties in composites, including the Flexure-After-Impact (FAI) protocol [17–19]. Studies using the FAI protocol are more limited than those using CAI, but FAI results confirm that increased impact energy leads to reductions in flexural modulus and strength [17–19]. However, no study to date has compared FAI and CAI testing protocols for damage modes and extent, nor mechanical sensitivity to impact damage.

Architecture of the impacted composites is also an important consideration when evaluating residual mechanical properties.

* Corresponding author at: Department of Aerospace Engineering, University of Illinois at Urbana-Champaign, 104 S. Wright St., Urbana, IL 61801, USA.

E-mail address: swhite@illinois.edu (S.R. White).

URL: <http://whitegroup.beckman.illinois.edu/> (S.R. White).

Composites made with woven fabrics have shown increased residual compressive strength and smaller delaminations than those made with unwoven unidirectional layers [20]. Through thickness stitching and z-pinning has also been employed to reduce delamination extent during impact [21]. More recently, three-dimensionally (3D) woven composite architectures have been utilized in structural composite applications. These composites contain through-thickness fiber tows which are co-woven with in-plane tows allowing insertion through the fabric thickness without rupturing in-plane fibers [22]. For reference, Fig. 1 depicts the unit cell of a common 2D and 3D composite fabric architecture. Despite multiple studies of the post-impact response of 3D composites, there have been few studies directly comparing composites made using newer 3D woven architectures to those fabricated with more classical 2D weaves [23].

The objective of this paper is to compare mechanical properties of 2D and 3D woven composites using the FAI and CAI protocols. Results of the two post-impact testing methods are first examined separately to investigate differences in the material response of 2D vs. 3D composite architectures. Then the test methods are compared and contrasted to elucidate the sensitivity of each testing protocol to impact damage. Finally, impact damage analysis from a companion paper [24] is combined with post-impact mechanical testing results to correlate damage formation to reductions in post-impact performance of both 2D and 3D composite architectures.

2. Materials and methods

2.1. Composite manufacturing

Composites with 3D woven reinforcement were fabricated from a single layer of 4.07 kg/m^2 (120 oz/yd^2) S2-glass orthogonal weave fabric (Textile Engineering and Manufacturing; Woonsocket, RI) consisting of 3 warp and 4 weft layers held by a through thickness penetrating Z-tow travelling in the warp direction. The warp and weft directions contain 3.0 tows/cm and 2.7 tows/cm, respectively. Additionally, composites with 2D woven reinforcement were made from 5 layers of 0.814 kg/m^2 (24 oz/yd^2) 1.97×1.97 tows/cm (5×5 tows/in.) plain woven S2-glass fabric (Owens Corning; Toledo, OH) arranged in a $[0]_5$ configuration, yielding the same fiber areal density ($4.07 \text{ kg/m}^2 = 5 \times 0.814 \text{ kg/m}^2$) as the 3D woven composites. Preforms were infused with epoxy resin by vacuum assisted resin transfer molding (VARTM). Epoxy resin components EPON 862 (diglycidyl ether of bisphenol F; Momentive, Inc.; Waterford, NY) and Epikure W (aromatic diamine; Momentive, Inc.) were obtained from Miller-Stephenson (Morton Grove, IL) and used as-received. Prior to infusion, components were mixed in a stoichiometric weight ratio of 100:26.4, heated for 30 min at $70 \text{ }^\circ\text{C}$ then degassed under vacuum for 2 h at $70 \text{ }^\circ\text{C}$. VARTM Infusion was carried out in a convection oven at $70 \text{ }^\circ\text{C}$ in order to lower the viscosity of the resin and facilitate

wetting of the fabric during infusion. Immediately after infusion the sample was raised to $121 \text{ }^\circ\text{C}$ at $3 \text{ }^\circ\text{C}/\text{min}$, held for 8 h, then cooled to room temperature at $1 \text{ }^\circ\text{C}/\text{min}$. 2D woven composites yielded an average thickness of $3.07 \pm 0.09 \text{ mm}$ and fiber volume fraction of $52.2 \pm 0.43\%$ calculated by the matrix burn-off method [23]. 3D woven composites had an average thickness of $3.52 \pm 0.06 \text{ mm}$ and fiber volume fraction of $47.3 \pm 0.24\%$. The lower fiber volume fraction in 3D samples is a result of interstitial regions present in the non-crimp orthogonally woven fiber preform which accommodate excess resin during infiltration. Plate samples were cut to $101 \times 101 \text{ mm}$. Beam specimens were cut to $20 \times 110 \text{ mm}$ with the warp direction aligned to the longitudinal axis of the beam.

2.2. Impact testing

2.2.1. Beam impact

Impact testing of beam samples was conducted on a drop-weight tower (Model 8250; Instron; Canton, MA). Samples were clamped in a fixed-fixed configuration with a free span of 40 mm and impacted in the center of the span across the entire width of the specimen with a cylindrical impact tup (25.4 mm radius of curvature). The tup configuration and the range of impact energies were selected to minimize fiber damage so that the effects of matrix damage and interface delamination could be isolated and investigated. Samples were impacted with a range of impact energies up to 25 J (Table 1).

2.2.2. Plate impact

Plate impact testing was conducted on a drop-weight tower (Dynatup 8200; Instron). Plate samples were circularly clamped (76 mm diameter free span) and impacted in the center with a hemi-spherically shaped impactor (25.4 mm radius of curvature). Samples were impacted with a range of energies up to 100 J (Table 2). A more detailed analysis of the effects of impactor geometry and boundary conditions on material response can be found in [24].

2.3. Flexure-After-Impact (FAI) testing (Beams)

Flexure testing was conducted on a load frame (Model 5984; Instron) with an affixed 5 kN load cell according to ASTM D6272. A schematic of the flexure testing apparatus is depicted in Fig. 2a. Samples were tested in four-point-bending at 2 mm/min crosshead displacement rate with an outer span of 80 mm and an inner span of 40 mm. All loading and support pins had a 6.35 mm radius of curvature. Center point deflection was measured by tracking the displacement of a spring loaded plunger in contact with the specimen during testing. Displacement of the plunger was measured with a non-contact video extensometer (Model AVE 2663-821; Instron). Hardware was controlled and data

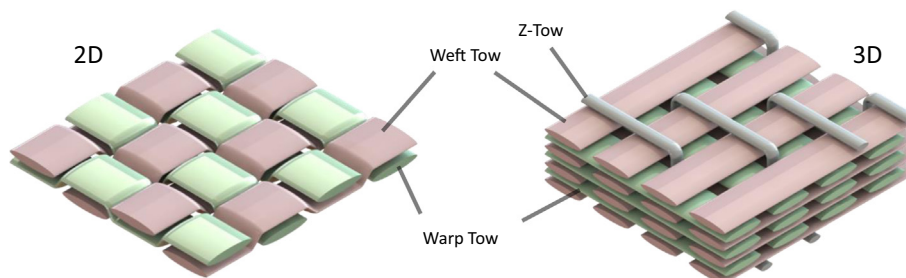


Fig. 1. Representative unit cells of 2D and 3D woven glass-fiber fabrics. The 2D fabric has an areal density of 814 g/m^2 and contains 2 tows/cm in both the warp and weft directions. The 3D fabric has an areal density of 4.07 kg/m^2 and contains 3 tows/cm in the warp direction and 2.7 tows/cm in the weft direction. Figure adopted from [24].

Table 1
Impact testing conditions for composite beam specimens.

Fabric architecture	Drop height, mm	Drop mass, kg	Impact energy, J	Impact velocity, m/s	No. of samples
2D	152	3.36	5.01	1.73	8
	304	3.36	10.0	2.44	8
	455	3.36	15.0	2.99	8
	759	3.36	25.0	3.86	8
3D	152	3.36	5.01	1.73	8
	304	3.36	10.0	2.44	8
	455	3.36	15.0	2.99	8
	759	3.36	25.0	3.86	8

Table 2
Impact testing conditions for composite plate specimens.

Fabric architecture	Drop height, mm	Drop mass, kg	Impact energy, J	Impact velocity, m/s	No. of samples
2D	600	4.34	25.5	3.43	8
	600	8.55	50.3	3.43	8
	600	12.79	75.3	3.43	8
	797	12.79	100	3.95	8
3D	600	4.34	25.5	3.43	8
	600	8.55	50.3	3.43	8
	600	12.79	75.3	3.43	8
	797	12.79	100	3.95	8

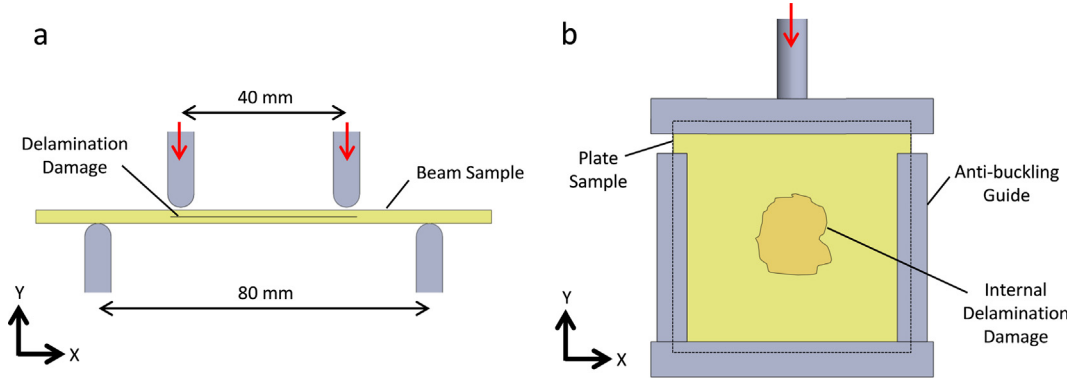


Fig. 2. Quasi-static testing of impacted beam and plate samples. (a) Apparatus for four-point flexure testing of impacted beam specimens. (b) Apparatus for compression testing of impacted plate specimens. (For interpretation of the references to color in this figure legend, the reader is referred to the web version of this article.)

was collected with Bluehill 3 (Instron) testing software. Samples were tested until fiber failure was visually observed across the width of the sample.

Maximum flexural stress in the beam occurs between the two central loading pins at the outer edges of the sample thickness and is calculated using Eulerian beam theory as

$$\sigma_f = 3PL/4wt^2 \quad (1)$$

where σ_f is the stress at the outer edge of the beam throughout the mid-span, P is the load, L is the support span, w is the width of the beam, and t is the thickness of the beam. Maximum flexural strain also occurs at the outer edge of the sample thickness throughout the mid-span and is calculated using

$$\varepsilon_f = 109\delta w/25L^2 \quad (2)$$

where ε_f is the maximum strain and δ is the deflection of the center of the beam. The secant flexural modulus, E_f , was then calculated between strain values of 0.003 and 0.005 in the elastic loading region using,

$$E_f = \frac{\sigma_f^{(\varepsilon_f=0.005)} - \sigma_f^{(\varepsilon_f=0.003)}}{0.005 - 0.003} \quad (3)$$

where $\sigma_f^{\varepsilon_f=0.003}$ and $\sigma_f^{\varepsilon_f=0.005}$ are the flexural stresses at flexural strain values of 0.003 and 0.005, respectively.

2.4. Compression-After-Impact (CAI) testing (Plates)

In-plane compression testing was conducted on a hydraulic test frame (Model 812; MTS Corporation; Eden Prairie, MN) at a cross-head speed of 1 mm/min according to ASTM D7137. Compression testing is depicted in Fig. 2b. During testing, samples were secured using an adapted CAI fixture modified to accommodate 101 × 101 mm plate specimens. This fixture utilizes anti-buckling edge guides on the sides, top, and bottom to prevent global buckling during testing. To ensure consistency of clamping conditions between tests, stainless steel shim stock (100 μm thickness) was placed between the sample and each guide while the guides were secured in the fixture. The shim was then removed prior to testing, leaving a 100 μm gap between the anti-buckling guides and the specimen on all sides. Samples were tested with the warp axis aligned to the loading direction (Y-direction in Fig. 2b). Panels were loaded until failure was observed across the width of the sample.

Compressive stress, σ_c , in the plate was calculated using

$$\sigma_c = P/wt \quad (4)$$

where P is the applied compressive load, w is the plate width, and t is the plate thickness. Compressive strain, ε_c , in the plate was calculated using

$$\varepsilon_c = \delta/L \quad (5)$$

where δ is the cross-head displacement and L is the length of the plate. The compressive tangent modulus as a function of strain, $E_c(\varepsilon_c)$, was calculated across the domain using

$$E_c(\varepsilon_c) = \frac{\sigma_c^{(\varepsilon_c+0.00125)} - \sigma_c^{\varepsilon_c}}{(\varepsilon_c + 0.00125) - \varepsilon_c} \quad (6)$$

where $\sigma_c^{\varepsilon_c}$ and $\sigma_c^{(\varepsilon_c+0.00125)}$ are the compressive stresses at strain values of ε_c and $(\varepsilon_c+0.00125)$ respectively. Finally, the maximum compressive tangent modulus, E_c^{max} , was defined as the maximum value of the compressive tangent modulus.

3. Results and discussion

3.1. Flexure-After-Impact (FAI) testing

Representative stress-strain curves for both 2D and 3D woven composite beam specimens during FAI testing are shown in Fig. 3. Both compressive strength and modulus are reduced as impact energy increases for both 2D and 3D composites. Failure is clearly identified in the stress-strain curve by the sudden reduction in load correlating with the emergence of visible and audible signs of failure. Undamaged samples or samples impacted with 5.0 J of energy commonly failed in transverse shear near one of the loading pins. Specimens impacted at higher energies all failed via compressive fiber buckling between the loading pins. Interestingly, the change in failure mode from shear-dominated to buckling-dominated correlated with the appearance of inter-ply delaminations during impact testing [24]. Images of the front and back faces of both 2D and 3D impacted (15 J) composite beam coupons after FAI testing are shown in Fig. 4. Buckling of the specimens on the compressive (top) face during flexure testing is clearly identified by the line of visible fiber failure that spans the width of each specimen.

Flexural strength as a function of impact energy is presented in Fig. 5a. As impact energy increases, both 2D and 3D composites exhibit reduced flexural strength. For both fiber architectures, samples impacted at 5.0 J do not exhibit appreciable damage and as a

result the flexural strength is relatively unaffected. However, at 10.0 J impact energy, significant delamination damage is introduced and flexural strength is severely reduced (ca. 40%). 2D woven composites show larger reductions in post-impact strength at the same impact energy compared to 3D architectures. The through thickness Z-tows in 3D composites limit delamination damage during impact through crack bridging and delamination crack deflection [24] ultimately leading to improved post-impact performance of 3D woven composites.

Flexural modulus as a function of impact energy is presented in Fig. 5b. At all impact energies, the modulus of 2D composites is greater than 3D composites as a result of the increased fiber volume fraction of 2D composites obtained during composite manufacture. Regardless, as impact energy increases, flexural modulus is reduced in both 2D and 3D composite samples at approximately the same rate. Again, reductions in flexural modulus correlate with the formation of inter-ply delaminations during impact further confirming that FAI testing results are sensitive to delamination damage from impact.

3.2. Compression-After-Impact (CAI) testing

Representative stress-strain curves for both 2D and 3D woven composite plate specimens during CAI testing are depicted in Fig. 6a and b, respectively. Failure is clearly identified by sudden reduction in the load corresponding to fiber kinking and shear band formation across the width (X-direction) of the specimen. Two large reductions in load are typically observed. Failure first runs in the X-direction from one edge of the specimen to the damage region in the center then later occurs on the other side during a second failure event to create a continuous damage path across the sample width through the entire impact damage area. Images of the front and back faces of both 2D and 3D impacted (75 J) composite coupons after CAI testing are shown in Fig. 7. Global buckling of the specimens from the compression testing is clearly identified by the visible fiber failure that spans the width and thickness of each specimen. Unlike beams tested during FAI, differences in the strain to failure, maximum strength, and modulus are not as easily distinguished across the various impact energies.

Compressive strength and maximum compressive tangent modulus as a function of impact energy are plotted in Fig. 8a and b, respectively. Unlike beam specimens during FAI testing, mechanical performance of plate specimens during CAI testing is much less sensitive to increases in impact energy. Even at the highest impact energies tested, reductions in post-impact strength were limited to 25% in the worst case (2D composites, 100 J). 3D

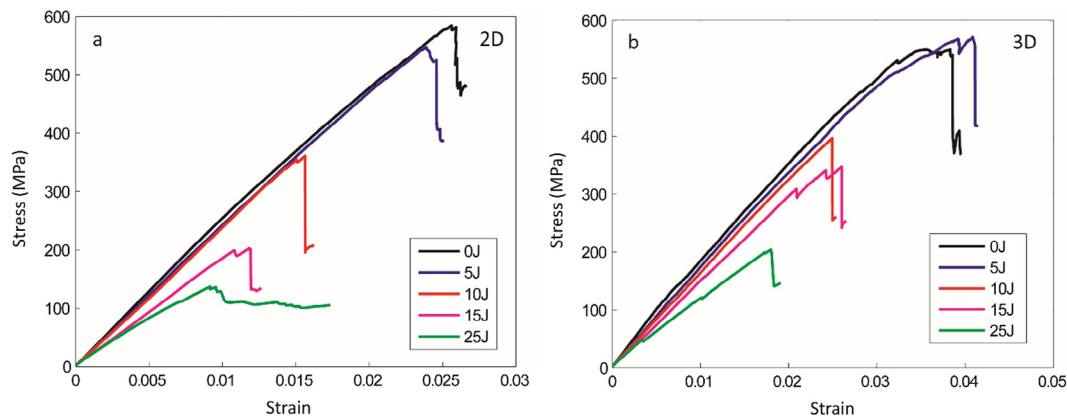


Fig. 3. Representative flexural stress vs. flexural strain during FAI testing. (a) 2D woven composite beams impacted over a range of impact energies (0–25 J). (b) 3D woven composite beams impacted over a range of impact energies (0–25 J). (For interpretation of the references to color in this figure legend, the reader is referred to the web version of this article.)

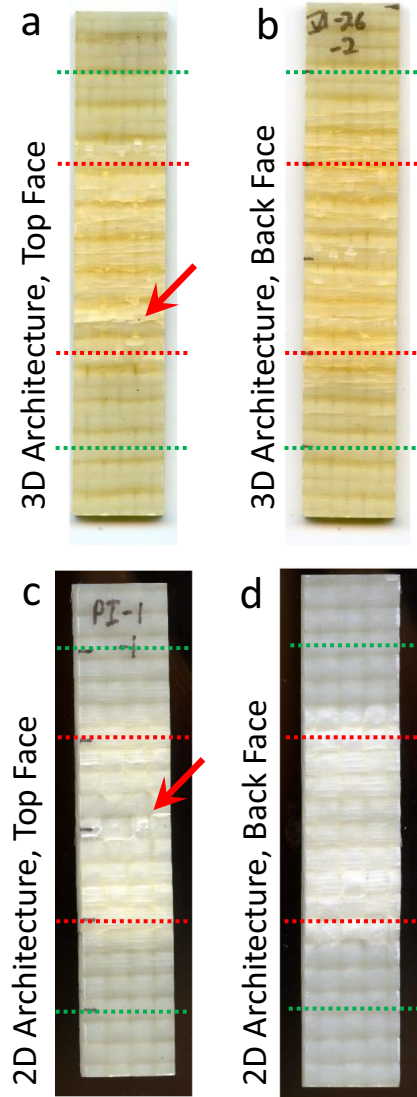


Fig. 4. Composite beam specimens after FAI testing. (a) Impacted face of a 3D composite specimen. (b) Back face of a 3D composite specimen. (c) Impacted face of a 2D composite specimen. (d) Back face of a 2D composite specimen. All specimens were impacted at 15 J. Red arrows highlight areas of local fiber buckling in the specimens on the top face. Red dashed lines are 40 mm apart, and represent the unclamped area during impact and the inner span during flexural testing. Green dashed lines are 80 mm apart and represent the outer span during flexural testing. (For interpretation of the references to color in this figure legend, the reader is referred to the web version of this article.)

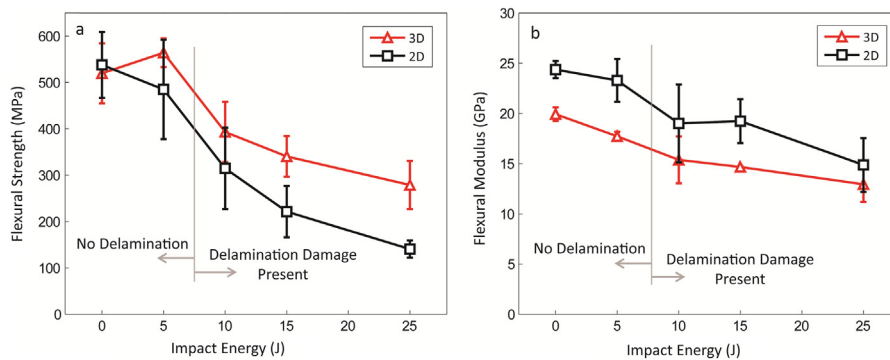


Fig. 5. Mechanical properties obtained by FAI testing. (a) Post-impact flexural strength as a function of impact energy for 2D and 3D woven composites. (b) Post-impact flexural modulus as a function of impact energy for 2D and 3D woven composites. Note that delamination damage is introduced at impact energies above 10 J. (For interpretation of the references to color in this figure legend, the reader is referred to the web version of this article.)

woven composites show no significant reduction in post-impact strength and modulus at any impact energy tested. Retention of mechanical properties in 3D woven composites is attributed to the through thickness reinforcement which binds fabric layers together to limit localized buckling in the vicinity of impact damaged regions.

3.3. Comparison of CAI and FAI protocols

CAI and FAI testing are directly compared by normalizing key parameters. Impact energy is first scaled by the unclamped sample volume for both CAI and FAI geometries, yielding impact energy density. For beams, this was calculated using

$$\bar{U} = U/Lwt_{beam} \quad (7)$$

and for plates this was calculated using

$$\bar{U} = 4U/\pi D^2 t_{plate} \quad (8)$$

where \bar{U} is the impact energy density, U is the impact energy, L is the unclamped beam span, w is the beam width, t_{beam} is the beam thickness, t_{plate} is the plate thickness, and D is the unclamped diameter of the plate. Post-impact mechanical properties are then normalized by undamaged properties of the same sample type. Normalized strength and moduli as a function of calculated impact energy density for 2D and 3D plates and beams subject to CAI and FAI testing are plotted in Fig. 9. Both 2D and 3D samples tested using the FAI protocol exhibit larger reductions in strength and modulus at the same impact energy density when compared to those tested using the CAI protocol. Impact of beams is more effective in inducing structural degradation in comparison to plate specimens. This difference is likely due to the fact that beam impact loads the full width of the specimen, and therefore any induced damage fully spans across the free edges of the specimen. In contrast, center impact on a clamped plate generates local damage at the plate center, remote from the specimen boundaries. Therefore, the global mechanical response of the composite is more sensitive to beam impact than plate impact.

3.4. Correlation of the extent of damage with post-impact mechanical performance

The analysis and characterization of impact damage for CAI and FAI testing [24] was used to correlate post-impact mechanical properties with total delamination length in Fig. 10. As delamination length increases, the normalized flexural strength decreases significantly for both 2D and 3D composites (Fig. 10a). Interestingly, the 3D composites have a higher residual strength at the

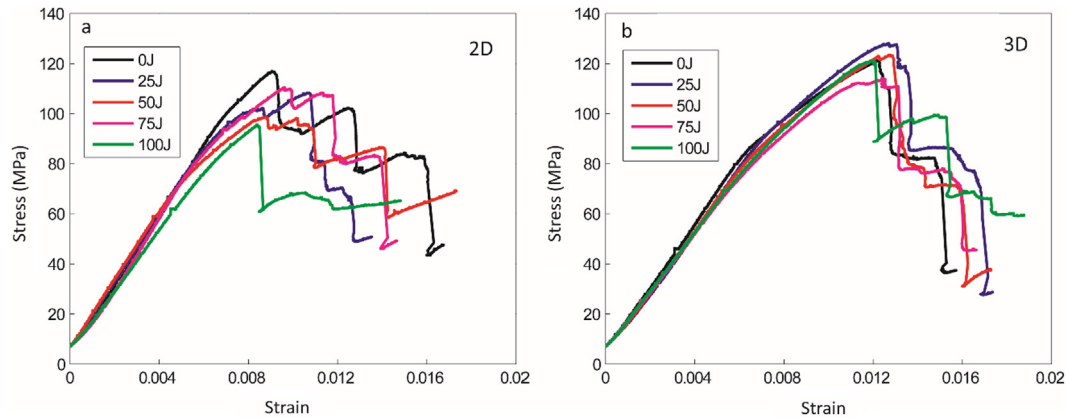


Fig. 6. Representative compressive stress vs. strain during CAI testing. (a) 2D woven composite plates impacted over a range of impact energies (0–100 J). (b) 3D woven composite plates impacted over a range of impact energies (0–100 J). (For interpretation of the references to color in this figure legend, the reader is referred to the web version of this article.)

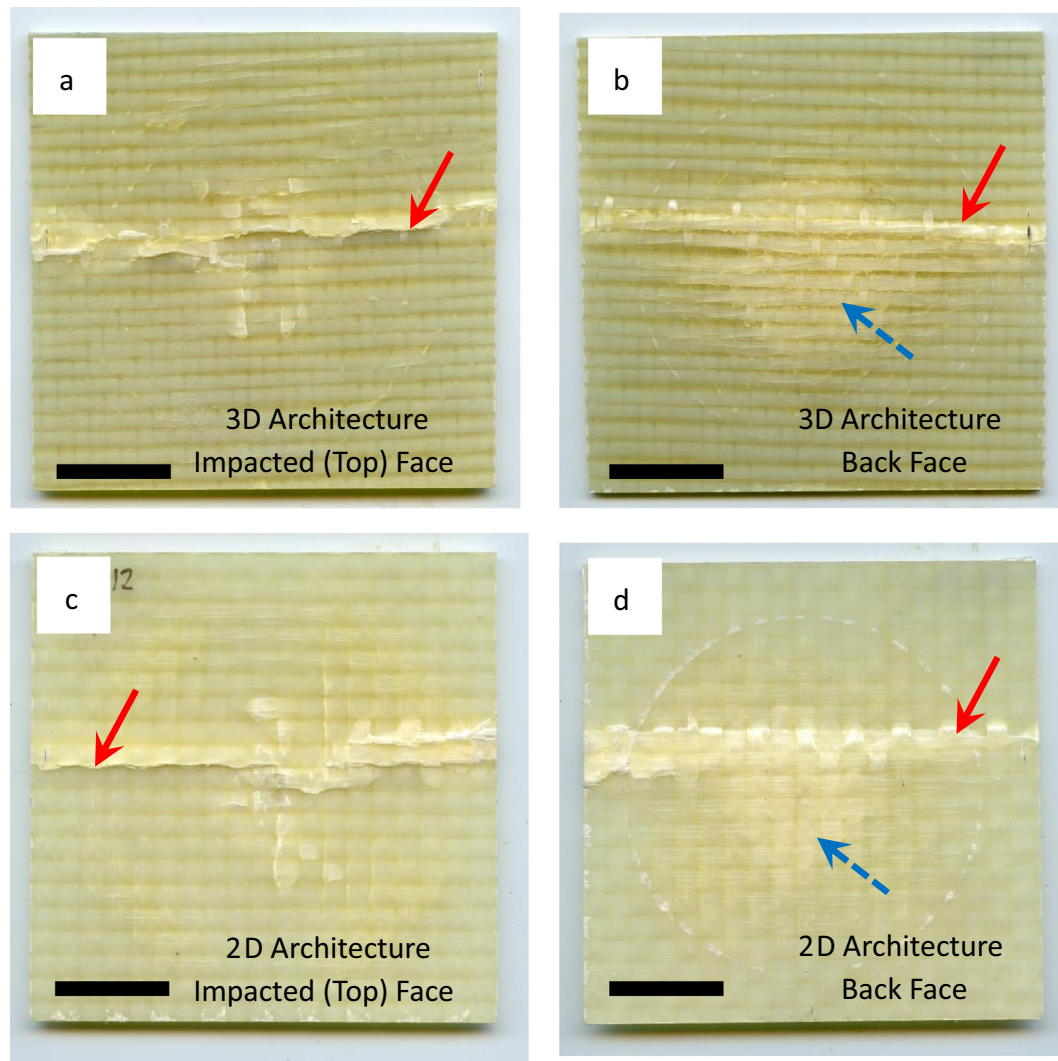


Fig. 7. Composite plate specimens after CAI testing. (a) Impacted face of a 3D composite specimen. (b) Back face of a 3D composite specimen. (c) Impacted face of a 2D composite specimen. (d) Back face of a 2D composite specimen. All specimens were impacted at 75 J. Red (solid) arrows show areas of global buckling in the specimens resulting from compression testing. Blue (dashed) arrows point to index mismatching on the back face of the specimens arising from internal delamination damage within the composite which occurred during out-of-plane impact. All scale bars are 25 mm. (For interpretation of the references to color in this figure legend, the reader is referred to the web version of this article.)

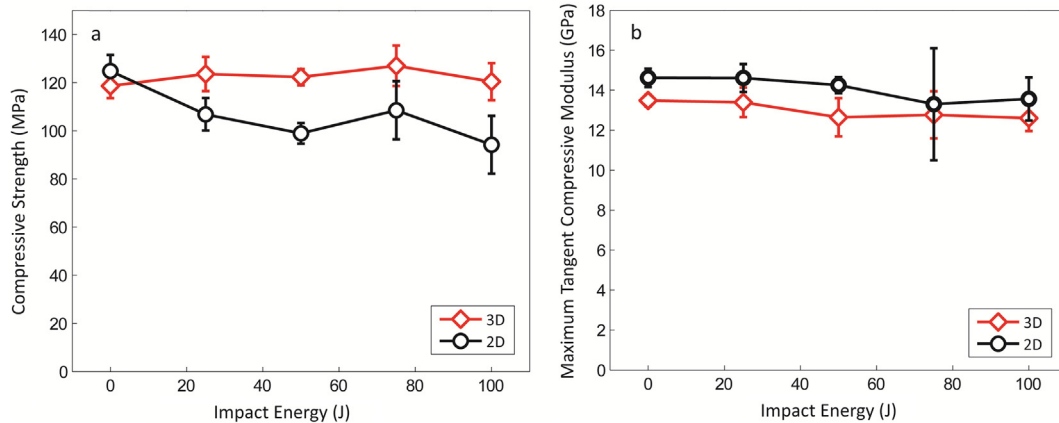


Fig. 8. Mechanical properties obtained by CAI testing. (a) Post-impact compressive strength as a function of impact energy for 2D and 3D woven composite plates. (b) Post-impact maximum tangent compressive modulus as a function of impact energy for 2D and 3D woven composite plates. Error bars represent one standard deviation of at least 5 samples. (For interpretation of the references to color in this figure legend, the reader is referred to the web version of this article.)

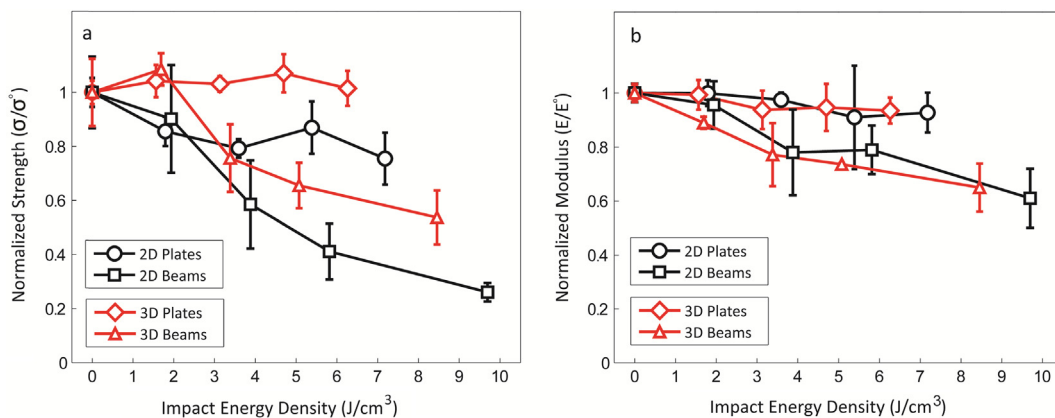


Fig. 9. Comparison of FAI and CAI results. (a) Normalized post-impact strength as a function of impact energy density for composite beams (FAI) and plates (CAI). (b) Normalized post-impact modulus as a function of impact energy density for composite beams (FAI) and plates (CAI). In both figures, error bars represent the standard deviation of at least 5 samples. (For interpretation of the references to color in this figure legend, the reader is referred to the web version of this article.)

same delamination length as 2D samples, likely because of the load sharing and resistance to buckling which occurs across delaminated regions in 3D composites as a result of Z-tow reinforcement. Similarly, the normalized flexural modulus of beam specimens decreases as a function of total delamination length for both 2D and 3D specimens (Fig. 10b).

Normalized compressive strength of plate specimens as a function of total delamination length is plotted in Fig. 10c. 2D woven composites show a reduced compressive stress with increasing delamination damage while 3D samples do not. Failure of plates during CAI occurs through local buckling mechanisms near the delaminated regions. 3D composites are more likely to resist localized buckling in the vicinity of the delaminations since the through thickness Z-tows provide lateral constraint to buckling. In contrast, 2D composites are unconstrained (through thickness) and as a result, are more sensitive to the introduction of delamination damage and have lower compressive strengths when compared to 3D composites containing the same measured delamination length. Finally, the normalized maximum tangential compressive modulus is plotted as a function of total delamination length in Fig. 10d. For both 2D and 3D composites, the modulus is insensitive to total delamination length. Since fibers are undamaged during impact, load sharing is maintained throughout the composite and the

compressive modulus is unaffected by the introduction of the delamination damage.

3.5. Selection of proper post-impact testing protocol

Ultimately, engineering discretion is required when selecting an impact testing protocol for specific applications. When flexural loading is important and one of the primary design drivers (e.g. aircraft wing panels and supports or wind turbine blades) then the FAI protocol may be the most suitable testing protocol, especially since it is more sensitive to pre-existing impact damage. However, for applications in which purely tensile/compressive loading is dominant (e.g. rocket motor casings or vehicle chassis) the CAI protocol may be more suitable without an unnecessary underestimation of residual properties.

4. Conclusions

In this paper, post-impact mechanical performance of 2D and 3D woven composites of identical areal densities and material components were evaluated using both Flexure-After-Impact (FAI) and Compression-After-Impact (CAI) testing protocols. Analysis of the CAI and FAI test results reveal that at the same

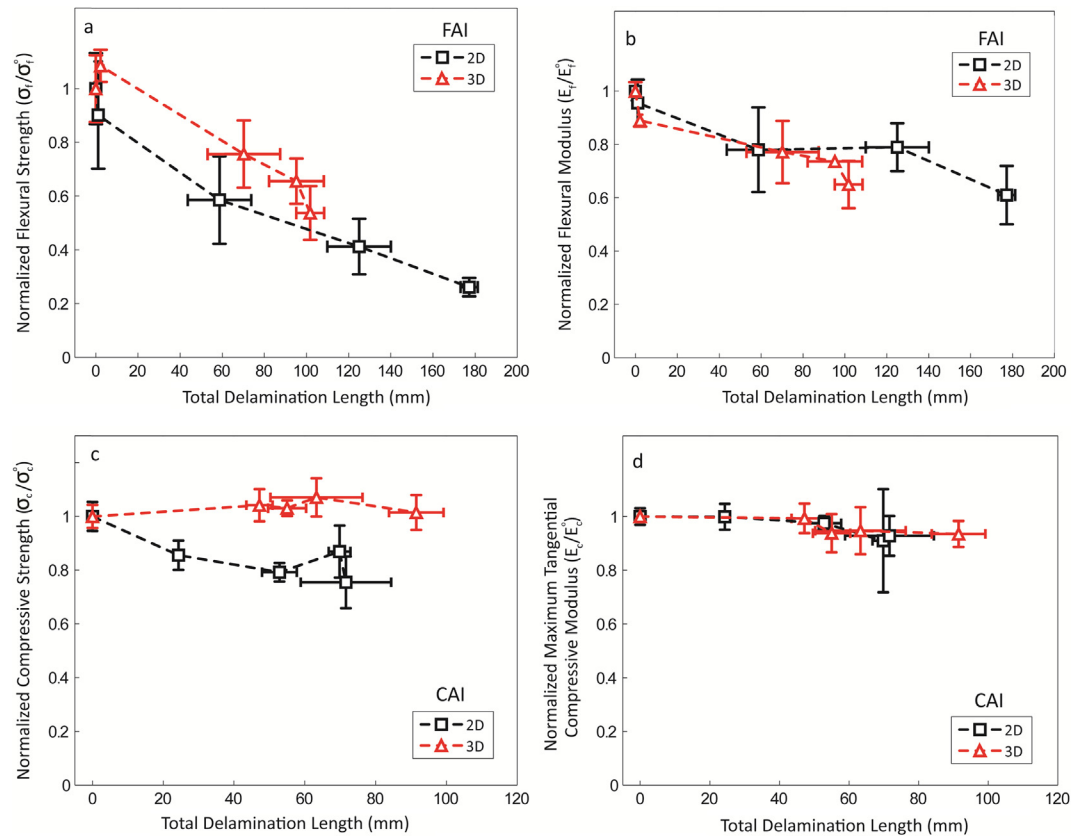


Fig. 10. Correlation of post-impact mechanical properties with total delamination length. (a, b) Normalized flexural strength and flexural moduli as a function of total delamination length for 2D and 3D woven composite beam specimens subject to the FAI testing protocol. (c, d) Normalized compressive strength and maximum tangential moduli as a function of total delamination length for 2D and 3D woven composite plate specimens subject to the CAI testing protocol. In all figures, vertical error bars represent the standard deviation of at least 5 measurements and horizontal error bars represent the standard deviation of at least 3 measurements. (For interpretation of the references to color in this figure legend, the reader is referred to the web version of this article.)

impact energy density, the FAI testing protocol results in larger reductions in mechanical performance compared to the CAI testing protocol. Post-impact flexural strength and flexural modulus of beam samples are more sensitive to delamination damage imparted during impact. Regardless of the testing protocol used, 2D composites had lower post-impact strengths than 3D composites impacted at the same impact energy, likely because Z-tows in 3D composites resist buckling failures during mechanical testing and limit delamination opening through crack bridging and delamination crack deflection during impact. The FAI testing protocol is an attractive alternative to CAI testing since FAI requires approximately 4.5x less material, does not require anti-buckling fixtures, and is more sensitive to the presence of delamination damage. However, discretion is required when selecting an impact testing protocol to ensure that the testing method accurately reflects the ultimate end-use of the material investigated.

Acknowledgements

The authors gratefully acknowledge funding support from the Army Research Laboratory (grant number W911NF-14-2-003) and Dr. Gavin Horn for assistance with compression-after-impact testing.

References

- [1] Caprino G. Residual strength prediction of impacted CFRP laminates. *J Compos Mater* 1984;18(6):508–18.
- [2] Cantwell WJ, Morton J. The impact resistance of composite materials – a review. *Composites* 1991;22(5):347–62.

- [3] Standard tests for toughened resin composites. NASA reference publication 1092. NASA Langley Research Center; 1982.
- [4] Curtis PT. CRAG test methods for the measurement of the engineering properties of fibre reinforced plastics. Royal aerospace establishment farnborough. United Kingdom; 1988.
- [5] Advanced composite compression tests. Boeing specification support standard BSS7620; 1982.
- [6] ASTM D7137. Standard test method for compressive residual strength properties of damaged polymer matrix composite plates.
- [7] Sela N, Ishai O. Interlaminar fracture toughness and toughening of laminated composite materials: a review. *Composites* 1989;20(5):423–35.
- [8] Hull D, Shi YB. Damage mechanism characterization in composite damage tolerance investigations. *Compos Struct* 1993;23(2):99–120.
- [9] Davies GAO, Hitchings D, Zhou G. Impact damage and residual strengths of woven fabric glass/polyester laminates. *Compos Part A: Appl Sci Manuf* 1996;27(12):1147–56.
- [10] Richardson MOW, Wisheart MJ. Review of low-velocity impact properties of composite materials. *Compos Part A: Appl Sci Manuf* 1996;27(12):1123–31.
- [11] Gao SL, Kim JK. Three-dimensional characterization of impact damage in CFRPs. *Key Eng Mater* 1998;141–143:35–54.
- [12] Shyr T-W, Pan Y-H. Impact resistance and damage characteristics of composite laminates. *Compos Struct* 2003;62(2):193–203.
- [13] Abrate S. Impact on laminated composite materials. *Appl Mech Rev* 1991;44(4):155–90.
- [14] Davies GAO, Zhang X, Zhou G, Watson S. Numerical modelling of impact damage. *Composites* 1994;25(5):342–50.
- [15] Elder DJ, Thomson RS, Nguyen MQ, Scott ML. Review of delamination predictive methods for low speed impact of composite laminates. *Compos Struct* 2004;66(1–4):677–83.
- [16] Tabiei A, Nilakantan G. Ballistic impact of dry woven fabric composites: a review. *Appl Mech Rev* 2008;61(1).
- [17] Cromer K, Gillespie JW, Keefe M. Effect of multiple non-coincident impacts on residual properties of glass/epoxy laminates. *J Reinf Plast Compos* 2012;31(12):815–27.
- [18] Santiuste C, Sanchez-Saez S, Barbero E. Residual flexural strength after low-velocity impact in glass/polyester composite beams. *Compos Struct* 2010;92(1):25–30.

- [19] Mouritz AP, Gallagher J, Goodwin AA. Flexural strength and interlaminar shear strength of stitched GRP laminates following repeated impacts. *Compos Sci Technol* 1997;57(5):509–22.
- [20] Cantwell W, Curtis P, Morton J. Post-impact fatigue performance of carbon fibre laminates with non-woven and mixed-woven layers. *Composites* 1983;14(3):301–5.
- [21] Mouritz AP, Cox BN. A mechanistic interpretation of the comparative in-plane mechanical properties of 3D woven, stitched and pinned composites. *Compos Part A: Appl Sci Manuf* 2010;41(6):709–28.
- [22] Bilisik K. Multiaxis three-dimensional weaving for composites: a review. *Text Res J* 2012;82(7):725–43.
- [23] Carlsson LA, Adams DF, Pipes RB. *Experimental characterization of advanced composite materials*. 4th ed. CRC Press; 2014.
- [24] Hart KR, Chia PXL, Sheridan LE, Wetzel ED, Sottos NR, White SR. Mechanisms and characterization of impact damage in 2D and 3D woven fiber-reinforced composites. *Compos Part A: Appl Sci Manuf* 2017. <http://dx.doi.org/10.1016/j.compositesa.2017.07.004>.